Science
AAAS

High-Detectivity Polymer Photodetectors with Spectral Response from 300 nm to 1450 nm
Xiong Gong, *et al.*
Science **325**, 1665 (2009);
DOI: 10.1126/science.1176706

Science (print ISSN 0036-8075; online ISSN 1095-9203) is published weekly, except the last week in December, by the American Association for the Advancement of Science, 1200 New York Avenue NW, Washington, DC 20005.

High-Detectivity Polymer Photodetectors with Spectral Response from 300 nm to 1450 nm

Xiong Gong,[1,2]* Minghong Tong,[1] Yangjun Xia,[3] Wanzhu Cai,[3] Ji Sun Moon,[1] Yong Cao,[3]* Gang Yu,[2] Chan-Long Shieh,[2] Boo Nilsson,[2] Alan J. Heeger[1,2]*

Sensing from the ultraviolet-visible to the infrared is critical for a variety of industrial and scientific applications. Today, gallium nitride–, silicon-, and indium gallium arsenide–based detectors are used for different sub-bands within the ultraviolet to near-infrared wavelength range. We demonstrate polymer photodetectors with broad spectral response (300 to 1450 nanometers) fabricated by using a small-band-gap semiconducting polymer blended with a fullerene derivative. Operating at room temperature, the polymer photodetectors exhibit detectivities greater than 10^{12} cm $Hz^{1/2}$/W and a linear dynamic range over 100 decibels. The self-assembled nanomorphology and device architecture result in high photodetectivity over this wide spectral range and reduce the dark current (and noise) to values well below dark currents obtained in narrow-band photodetectors made with inorganic semiconductors.

Sensing from the ultraviolet (UV)–visible to the infrared is critical for a variety of industrial and scientific applications, including image sensing, communications, environmental monitoring, remote control, day- and night-time surveillance, and chemical/biological sensing (*1*–*4*). Today, separate sensors or materials are required for different sub-bands within the UV to near-infrared (NIR) wavelength (λ) range. In general, GaN-, Si-, and InGaAs-based detectors are used for the three important sub-bands, 0.25 μm to 0.4 μm (UV), 0.45 μm to 0.8 μm (visible) and 0.9 μm to 1.7 μm (NIR), respectively. The detectivities of silicon photodetectors are ~4×10^{12} Jones (1 Jones = 1 cm $Hz^{1/2}$/W). The typical detectivities of InGaAs photodetectors are greater than 10^{12} Jones when cooled to 4.2 K. It would be advantageous to have a low-cost multicolor photodetector system with high quantum efficiency, high sensitivity, and high speed over the broad spectral range from the UV to the NIR and which does not require cooling to obtain high detectivity.

Colloidal inorganic semiconductor quantum dots (PbS) were used to fabricate NIR photodetectors onto gold interdigitated electrodes (*5*, *6*). These NIR photodetectors showed photoconductive gain and photoresponse out to 1450 nm. However, the quantum dot NIR photodetectors were fabricated using the "in-plane" structure (two electrodes and the PbS quantum dot semiconductor all in one plane) with electrode spacing > 5 μm. As a result, the required driving voltage is too high (>40 V) to be used with any commercially available thin film transistors (TFTs) (*6*).

These limitations substantially restrict the application of inorganic photodetectors in day- and night-time surveillance and chemical/biological sensing where high-speed and low-power photodetectors are desired.

After the initial discovery of ultrafast photoinduced electron transfer from semiconducting polymers to fullerenes (*7*), polymer photodetectors (PPDs) with fast temporal response and high sensitivity were reported with spectral response from 400 nm to 900 nm (*8*–*12*). However, there is no report on PPDs with photoresponse spanning the full range from the UV-visible to the NIR. We have successfully demonstrated PPDs with photoresponsivity from the UV to 1450 nm, fabricated by spin-casting the small-band-gap conjugated polymer, poly(5,7-bis(4-decanyl-2-thienyl)-thieno(3,4-*b*)diathiazole-thiophene-2,5) (PDDTT), blended with (6,6)-phenyl-C_{61}-butyric acid methyl ester ($PC_{60}BM$).

The molecular structures of PDDTT and $PC_{60}BM$ are shown in Fig. 1A. PDDTT was synthesized using the Stille coupling reaction (*13*–*15*). Figure 1B shows the normalized UV-visible absorption spectra of thin films of pristine PDDTT, pristine $PC_{60}BM$, and PDDTT:$PC_{60}BM$ composites. The inset shows the absorption spectra in the short-wavelength range from 300 nm to 500 nm. Pristine PDDTT thin films exhibit two absorption peaks, at ~480 nm and ~860 nm. The onset of the PDDTT absorption is at λ = 1450 nm, in good agreement with the calculated theoretical value obtained from geometry-optimized density functional calculations [see Supporting Online Material SOM)] (*16*–*18*). The onset wavelength at 1450 nm is the result of the small single-chain energy gap of PDDTT (~0.8 eV), which is sensitive to an increase (or decrease) in conjugation length (*19*, *20*). The addition of 50% w/w of $PC_{60}BM$ does not substantially alter the absorption properties of PDDTT; the new spectral feature that appears between 350 nm and 500 nm in the spectrum of the PDDTT:$PC_{60}BM$ composites originates from $PC_{60}BM$.

The energy levels [highest occupied molecular orbital (HOMO) and lowest unoccupied molecular orbital (LUMO)] of PDDTT and $PC_{60}BM$ were determined by cyclic voltammetry. The results are shown in Fig. 1C along with the work functions of indium tin oxide (ITO) and aluminum (Al). Figure 1C also shows the energy diagrams for poly[3-3′(vinylcarbazole)] (PVK), C_{60}, polystyrene-N,N-diphenyl-N,N-bis(4-n-butylphenyl)-(1,10-biphenyl)-4,4-diamine-perfluorocyclobutane (PS-TPD-PFCB) and the work function of poly(3,4-ethylenedioxythiophene):poly(styrenesulfonate) (PEDOT:PSS). (The molecular structures of PVK, C_{60}, and PS-TPD-PFCB are shown in the SOM.) Based on the energy-level diagrams shown in Fig. 1C, charge-separated carriers can be efficiently generated by photo-induced electron transfer and subsequently transported via the bulk heterojunction nanomorphology to opposite electrodes. Any barriers to charge collection at the electrodes are small as a result of the small energy differences at the PDDTT-ITO interface and at the $PC_{60}BM$-Al interface.

The short-circuit current observed from ITO/PEDOT/PDDTT:$PC_{60}BM$/Al devices (Fig. 2A) is ~200 times as high as that from ITO/PEDOT/PDDTT/Al devices, indicating that mobile carriers are photogenerated by ultrafast photoinduced electron transfer at a PDDTT:$PC_{60}BM$ heterojunction (*7*, *21*). Time-resolved photoinduced absorption and transient photoconductivity were carried out to verify the ultrafast photoinduced charge transfer and to verify the generation of long-lived mobile carriers (see the results in the SOM). We note that because of the high absorption coefficient over this broad absorption spectral region, PDDTT is a promising semiconducting polymer for use in bulk heterojunction photovoltaic cells. The absorption spectrum of PDDTT:$PC_{60}BM$ covers nearly the entire solar emission spectrum.

To achieve high sensitivity, we fabricated the polymer photodetector using phase-separated bulk heterojunction blends. The PDDTT:$PC_{60}BM$ bulk heterojunction active layer (Fig. 2A) forms interpenetrating bicontinuous donor and acceptor networks. Figure 2A shows the device architecture. The composition of PEDOT:PSS (as formulated for use in PPDs) and the details of the device fabrication are given in the SOM. A tungsten lamp was used as the light source to measure the PPDs' photoresponsivity. Figure 2B shows the current-voltage (*I*-*V*) characteristics measured in the dark and under illumination with λ = 800 nm with intensity of 0.22 mW/cm^2. The photodetector diode exhibits a rectification ratio of ~10^3 (at ±1 V bias) in the dark. To obtain the responsivity (*R* in A/W), the ratio of photocurrent to incident-light intensity must be measured

$$R = J_{ph}/L_{light} \quad (1)$$

where J_{ph} is the photocurrent and L_{light} is the incident light intensity. Thus, we measured the

[1]Center of Polymers and Organic Solids, University of California, Santa Barbara, CA 93106, USA. [2]CBrite Inc., Goleta, CA 93117, USA. [3]Institute of Polymer Optoelectronic Materials and Devices, South China University of Technology, Guangzhou 510640, P. R. China.

*To whom correspondence should be addressed. E-mail: xgong@physics.ucsb.edu (X.G.); poycao@scut.edu.cn (Y.C.); ajhe@physics.ucsb.edu (A.J.H)

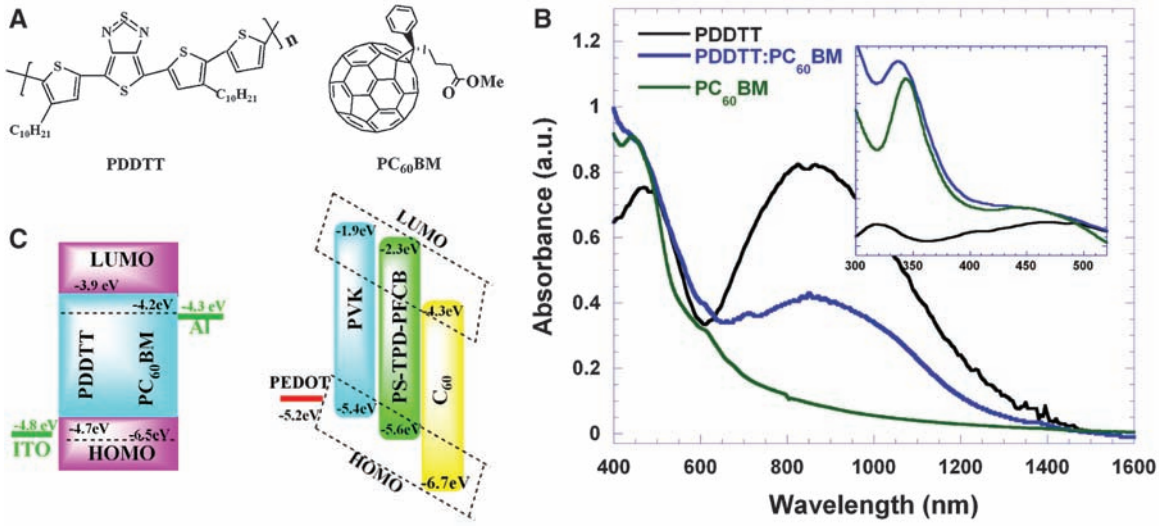

Fig. 1. (**A**) Molecular structures of PDDTT and $PC_{60}BM$. (**B**) Absorption spectra of thin films: pristine PDDTT, pristine $PC_{60}BM$, and PDDTT:$PC_{60}BM$ bulk heterojunction composites. Inset shows the absorption spectra from 300 to 500 nm. (**C**) Energy-level diagrams of PDDTT, $PC_{60}BM$, PVK, PS-TPD-PFCB, C_{60}, ITO, PEDOT, and Al.

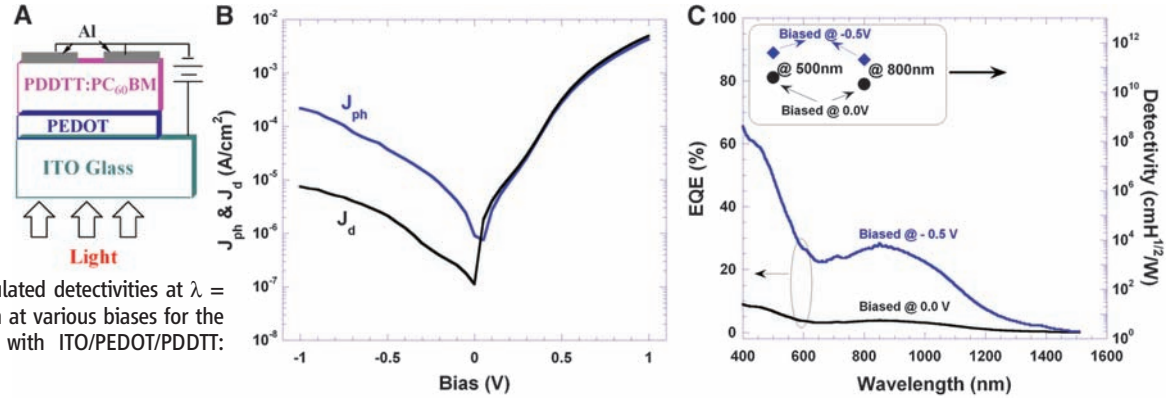

Fig. 2. (**A**) Schematic layout of the ITO/PEDOT/PDDTT:$PC_{60}BM$/Al photodetector on glass substrate. (**B**) Current-voltage (*I-V*) characteristics of polymer photodetectors measured in the dark and under illumination with $\lambda = 800$ nm. (**C**) EQE versus wavelength and calculated detectivities at $\lambda = 500$ nm and $\lambda = 800$ nm at various biases for the polymer photodetectors with ITO/PEDOT/PDDTT:$PC_{60}BM$/Al architecture.

external quantum efficiency (EQE) under short-circuit conditions and under reverse bias using the lock-in amplifier technique. The data are presented in Fig. 2C. The similar profiles of absorption and EQE spectra of PDDTT:$PC_{60}BM$ (Figs. 1B and 2C) demonstrate that photons absorbed by PDDTT in the NIR do indeed contribute to the photocurrent. At $\lambda = 800$ nm, the EQE is 26% electron per photon. Accordingly, R is calculated using Eq. 1 to be 0.17 A/W.

The photodetector figure of merit is the noise equivalent power (NEP), i.e., the minimum impinging optical power that a detector can distinguish from the noise.

$$\mathrm{NEP} = (A\Delta f)^{1/2}/D^* \quad (2)$$

where A is the effective area of the detector in cm^2, Δf is the electrical bandwidth in Hz, and D* is the detectivity measured in units of Jones. D^* is given by the following

$$D^* = (A\Delta f)^{1/2}R/i_n \quad (3)$$

where R the responsivity in A/W measured under the same conditions as the noise current i_n (in amperes).

There are three contributions to the noise that limit D^* (*22*, *23*): shot noise from dark current, Johnson noise, and thermal fluctuation "flicker" noise. If, as expected, the shot noise from the dark current is the major contribution, the detectivity can be expressed as

$$D^* = R/(2qJ_d)^{1/2} = (J_{\mathrm{ph}}/L_{\mathrm{light}})/(2qJ_d)^{1/2} \quad (4)$$

where q is the absolute value of electron charge (1.6×10^{-19} Coulombs) and J_d is the dark current. Detectivities were calculated (based on the measured photocurrent, dark current, and incident light intensity) using Eq. 4 at $\lambda = 500$ nm and $\lambda = 800$ nm for the PPDs with the ITO/PEDOT/PDDTT:$PC_{60}BM$/Al structure.

At zero bias, the calculated detectivities are $D^* = 3.9 \times 10^{10}$ Jones and 2.1×10^{10} Jones for PPDs under the illumination at 500 nm with light intensity of 0.28 mW/cm^2 and 800 nm with light intensity of 0.22 mW/cm^2, respectively. With a bias at –500 mV, $D^* = 3.9 \times 10^{10}$ Jones and 2.1×10^{10} Jones for illumination at 500 nm and 800 nm, respectively.

As shown below, these modest detectivities are limited by the high dark current. In the bulk heterojunction blend, the dark current is determined by the energy difference, E_{PF}, between the HOMO (top of the valence or π-band) of PDDTT and the LUMO of $PC_{60}BM$. The dark current is given by the diode equation:

$$J_{\mathrm{dark}} = J_0 exp(eV/nkT) \quad (5)$$

where J_0 is the dark saturation current that is dependent on E_{PF}, V is the applied voltage across photodetector, e is absolute value of electron charge, k is Boltzmann's constant, T is absolute temperature (K), and n is the ideality factor.

To minimize the dark current, we fabricated various polymer photodetectors with different multilayer structures. The general concept is to create blocking electrodes that suppress the thermally generated dark current. Polymer photodetectors with the following structures were characterized in detail:

(i) PPD1: ITO/PDDTT:$PC_{60}BM$/Al

(ii) PPD2: ITO/PEDOT/PDDTT:$PC_{60}BM$/Al

(iii) PPD3: ITO/PEDOT/PDDTT:$PC_{60}BM$/C_{60}/Al

(iv) PPD4: ITO/PEDOT/PVK/PDDTT:$PC_{60}BM$/C_{60}/Al

(v) PPD5: ITO/PEDOT/PS-TPD-PFCB/PDDTT:$PC_{60}BM$/C_{60}/Al

Atomic force microscopy images clearly indicated that the film quality of PDDTT:$PC_{60}BM$ directly on top of ITO was poor. Film quality of PDDTT:$PC_{60}BM$ on top of a PEDOT planarization layer (cast onto top of ITO) was better (see SOM).

In Fig. 3A, we plot the measured photocurrent and dark current at –100 mV bias for each

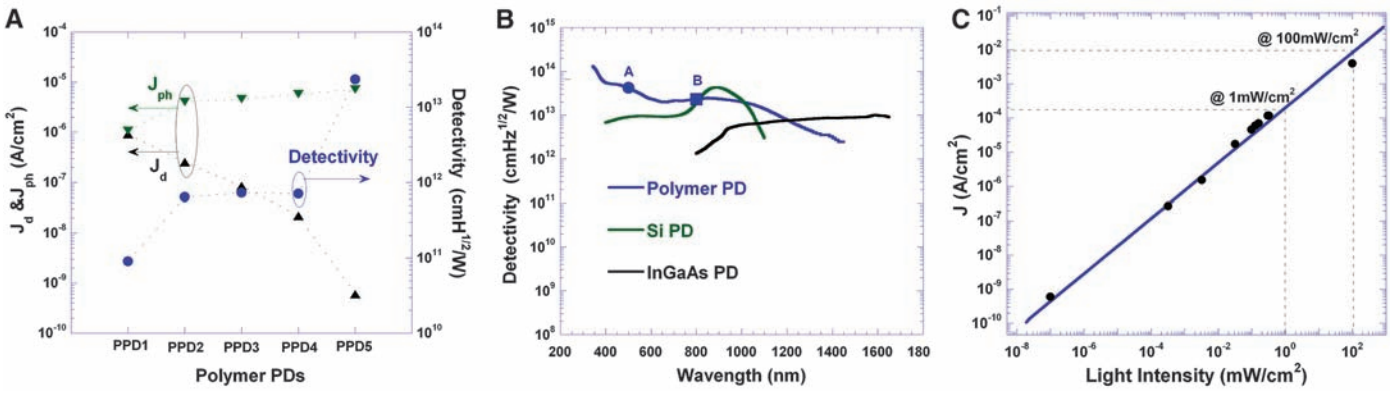

Fig. 3. (**A**) Photocurrent, dark current, and calculated detectivity at λ = 800 nm for each of the PPDs structures biased at −100 mV. (**B**) Detectivities of Si photodetector, InGaAs photodetector, and polymer photodetector versus wavelength. The high detectivities (10^{12} Jones) of the InGaAs photodetectors require cooling the devices to 4.2 K. The detectivities of the PPDs (ITO/PS-TPD-PFCB/PDDTT:$PC_{60}BM$/C_{60}/Al) were calculated at λ = 500 nm (point A) and λ = 800 nm (point B) biased at −100 mV. The solid blue curve was obtained from the measured photoresponsivity data with absolute magnitude determined by points A and B. (**C**) LDR of the polymer photodetectors with ITO/PS-TPD-PFCB/PDDTT:$PC_{60}BM$/C_{60}/Al architecture.

of the PPD structures. Using these values, the detectivities at 800 nm were calculated using the equations given above with the assumption that the detectivity is limited by dark current. The best results (highest photocurrent, lowest dark current, and highest detectivity) were obtained with the PPD5 structure. As described above, a high dark current is expected from PPD1 and PPD2 devices because PPDDTT is a narrow bandgap semiconducting polymer and E_{PF} is relatively small. In PPD3 and PPD4, a thin layer of C_{60} blocks photogenerated holes from moving into the Al cathode and a thin layer of PVK blocks photogenerated electrons from moving into the ITO anode. As a result, higher photocurrents and lower dark currents were observed. Even better results were obtained (PPD5) by replacing the nonconjugated PVK, with the high-conductivity, cross-linkable, low-HOMO, hole-transporting polymer (electron blocking) PS-TPD-PFCB (*24*, *25*). Figure 3A also shows the calculated detectivities at −100mV bias for each of the PPDs when illuminated at 800 nm with a light intensity of 0.22 mW/cm^2. The results shown in Fig. 3A clearly demonstrate that achieving high detectivity requires not only high photoresponsivity (high photocurrent) but also low noise (low dark current).

In Fig. 3B, we compare the detectivities of PPDs with detectivities of Si and InGaAs photodetectors. As in Fig. 3A, the detectivities of PPD5 were calculated at 500 nm (4.2×10^{13} Jones) and 800 nm (2.3×10^{13} Jones) using the equations given above, with the assumption that the detectivity is limited by dark current. By combining the calculated detectivities at 800 nm with the photoresponsivity data, the PPDs' detectivity values were obtained over the entire spectral range (Fig. 3B). Operating at room temperature, the optimized PPDs exhibited spectral response from 300 nm to 1450 nm, with detectivity greater than 10^{13} Jones at wavelengths from 300 nm to 1150 nm and greater than 10^{12} Jones from 1150 nm to 1450 nm. The detectivity (Fig. 3B) of the PPDs is comparable to or even better than those from Si and InGaAs photodetectors. Moreover, the PPD covers a significantly broader spectral range than Si or InGaAs photodetectors.

Another figure of merit for photodetectors is the linear dynamic range (LDR) or photosensitivity linearity (typically quoted in dB). LDR is given by

$$\mathrm{LDR} = 20\log(J^*_{ph}/J_d) \qquad (6)$$

where J^*_{ph} is the photocurrent, measured at light intensity of 1 mW/cm^2. Figure 3C shows the photocurrent versus the light intensity for PPD5. Under illumination at λ = 800 nm, the LDR for PPD5 is more than 100 dB, which is close to that of a Si photodetector (120 dB) and significantly higher than that obtained from InGaAs photodetectors (66 dB).

The results presented here demonstrate that the performance parameters of polymer photodetectors based on PDDTT are comparable to or even better than photodetectors fabricated from inorganic materials. The achievement of high-performance polymer photodetectors implies that semiconducting polymers can be used in a variety of possible sensor applications. The photoresponsivity and detectivity results open exciting opportunities for the creation of detectors with unusually wide spectral range and for the fabrication of high-resolution detector arrays for optical communications, chemical/biological sensing, and day- and night-time surveillance.

References and Notes

1. A. Rogalski, J. Antoszewski, L. Faraone, *J. Appl. Phys.* **105**, 091101 (2009).
2. M. Ettenberg, *Adv. Imaging* **20**, 29 (2005).
3. E. H. Sargent, *Adv. Mater.* **17**, 515 (2005).
4. S. Kim *et al.*, *Nat. Biotechnol.* **22**, 93 (2004).
5. S. A. Mcdonald, G. Konstantatos, S. G. Zhang, P. W. Cyr, E. J. D. Klem, L. Levina, E. H. Sargent, *Nat. Mater.* **4**, 138 (2005).
6. G. Konstantatos *et al.*, *Nature* **442**, 180 (2006).
7. N. S. Sariciftci, L. Simliowitz, F. Wudl, A. J. Heeger, *Science* **258**, 1474 (1992).
8. G. Yu, J. Gao, J. C. Hummelen, F. Wudl, A. J. Heeger, *Science* **270**, 1789 (1995).
9. G. Yu, J. Wang, J. McElvain, A. J. Heeger, *Adv. Mater.* **10**, 1431 (1998).
10. P. Schilinsky, C. Waldauf, C. J. Barabec, *Appl. Phys. Lett.* **81**, 3885 (2002).
11. P. Peumans, V. Bulovic, S. R. Forrest, *Appl. Phys. Lett.* **76**, 3855 (2000).
12. G. A. O'Brien, A. J. Quinn, D. A. Tanner, G. Redmond, *Adv. Mater.* **18**, 2379 (2006).
13. Y. J. Xia *et al.*, *Appl. Phys. Lett.* **89**, 081106 (2006).
14. S. Tanaka, Y. Yamashita, *Synth. Met.* **69**, 599 (1995).
15. Q. Hou *et al.*, *Macromolecules* **37**, 6299 (2004).
16. J. Seixas de Melo, M. Silva Luís, G. Arnaut Luís, R. S. Becker, *J. Chem. Phys.* **111**, 5427 (1999).
17. G. R. Hutchison *et al.*, *Phys. Rev. B* **68**, 035204 (2003).
18. G. R. Hutchison, M. A. Ratner, T. J. Marks, *J. Am. Chem. Soc.* **127**, 2339 (2005).
19. T. Chen, X. Wu, R. D. Rieke, *J. Am. Chem. Soc.* **117**, 233 (1995).
20. H. Saadeh, T. Goodson III, L. P. Yu, *Macromolecules* **30**, 4608 (1997).
21. C. H. Lee *et al.*, *Phys. Rev. B* **48**, 15425 (1993).
22. A. R. Jha, *Infrared Technology* (Wiley, New York, 2000.), pp. 245–359.
23. P. Bhattacharya, *Semiconductor Optoelectronics Device* (Prentice-Hall, Upper Saddle River, NJ, 1997), pp. 345–367.
24. X. Gong, D. Moses, A. J. Heeger, S. Liu, A. K.-Y. Jen, *Appl. Phys. Lett.* **83**, 183 (2003).
25. Y. Shao, X. Gong, A. J. Heeger, M. Liu, A. K.-Y. Jen, *Adv. Mater.* **21**, 1972 (2009).

26. This research was partially supported by the Defense Advanced Research Projects Agency Hemispheric Array Detectors for Imaging Program (D. Shenoy, Program Officer). The authors are grateful to A. Jen at the University of Washington for providing PS-TPD-PFCB. X. Gong thanks S. H. Park and N. Coates for assistance in optical measurements. The South China University of Technology thanks the National Science Foundation of China (50433030 and 50828301).

Supporting Online Material

www.sciencemag.org/cgi/content/full/1176706/DC1
Materials and Methods
Figs. S1 to S3
Table S1
References

22 May 2009; accepted 28 July 2009
Published online 13 August 2009;
10.1126/science.1176706
Include this information when citing this paper.